Extracellular-vesicle catch-and-release isolation system using a net-charge invertible curvature-sensing peptide

Kenichi Kawano[a, *], Yuki Kuzuma[a], Koichi Yoshio[a], Kenta Hosokawa[a], Yuuto Oosugi[a], Takahiro Fujiwara[b], Fumiaki Yokoyama[c], and Katsumi Matsuzaki[a]

a) Graduate School of Pharmaceutical Sciences, Kyoto University, 46-29 Yoshida-Shimoadachi-cho, Sakyo-ku, Kyoto 606-8501, Japan

b) Institute for Integrated Cell-Material Sciences (WPI-iCeMS), Kyoto University, Yoshida-Honmachi, Sakyo-ku, Kyoto 606-8501, Japan

c) Graduate School of Science, The University of Tokyo, 7-3-1 Hongo, Bunkyo-ku, Tokyo 113-0033, Japan

KEYWORDS: extracellular vesicles, curvature-sensing peptides, biosensor, EV-CaRiS, single-particle imaging, EV isolation

ABSTRACT: Extracellular vesicles (EVs) carry various informative components, including signaling proteins, transcriptional regulators, lipids, and nucleic acids. These components are utilized for cell-cell communication between the donor and recipient cells. EVs have shown great promise as pharmaceutical-targeting vesicles and have attracted the attention of researchers in the fields of biological and medical science because of their importance as diagnostic and prognostic markers. However, the isolation and purification of EVs from cell-cultured media remain challenging. Ultracentrifugation is the most widely used method, whereas it requires specialized and expensive equipment. In the present study, we proposed a novel methodology to isolate EVs using a simple and convenient method, *i.e.,* an EV catch-and-release isolation system (EV-CaRiS) using a net-charge invertible curvature-sensing peptide (NIC). Curvature-sensing peptides recognize vesicles by binding to lipid-packing defects on highly curved membranes, regardless of the expression levels of biomarkers. NIC was newly designed to reversibly capture and release EVs in a pH-dependent manner. NIC allowed us to achieve reproducible EV isolation from three human cell lines on resin using a batch method and single-particle imaging of EVs containing the ubiquitous exosome markers CD63 and CD81 by total internal reflection fluorescence microscopy (TIRFM). EV-CaRiS was demonstrated as a simple and convenient methodology for EV isolation, and NIC is promising for applications in the single-particle analysis of EVs.

INTRODUCTION

Extracellular vesicles (EVs) are biogenic lipidic nanoparticles secreted by most mammalian cells and are known to be involved in cell-cell communication both proximally and distally[1, 2]. EVs carry biomarkers and signaling molecules involved in diverse human diseases[3, 4]; therefore, they show great promise as pharmaceutical targeting vesicles and as sources of diagnostic and prognostic markers[5]. The subtypes of EVs released from mammalian cells can be separated into the following categories: the relatively smaller and homogeneous size class with diameters of 50–200 nm (known as small EVs including "exosomes") and the larger and heterogeneous size class with diameters of 150 to ~1,500 nm (known as "microvesicles")[6, 7]. Small EVs with diameters of 50–200 nm commonly have high membrane curvature but the expression levels of biomarkers herein depend on the cell line and culture conditions.

Although ultracentrifugation (UC) is the major strategy for isolating EVs from cell-cultured media by the stepwise separation depending on sedimentation coefficients, the purity of small EVs isolated by UC is relatively low because of its low selectivity and contamination with protein complexes of high molecular mass[6, 8]. Moreover, the conventional UC method requires totally 4–6 h or more for EV isolation from a large amount of cell-cultured media[8-10]. Therefore, no gold standard methodology has been developed to date that allows researchers to reproducibly isolate EVs from small-scale media by a simple method in a short time using general experimental equipment found in ordinary laboratories.

For EV detection, we have previously created a curvature-sensing peptide, nFAAV5[11, 12], based on the sequence of sorting nexin protein 1[13] of the Bin/Amphiphysin/Rvs protein family. nFAAV5 selectively binds to bacterial EVs with high sensitivity even in the presence of EV-secretory cells in cultured media. We have developed a simple and rapid method for *in situ* vesicle detection in cell-cultured media without cell removal and EV purification[14].

In this study, to isolate small EVs using a simple and convenient method, we propose a novel methodology, an EV catch-and-release isolation system (EV-CaRiS) using a net-charge invertible curvature-sensing peptide (NIC). Curvature-sensing peptides recognize vesicles by binding to lipid-packing defects on highly curved membranes, regardless of the expression levels of biomarkers. NIC was designed for the catch-and-release of EVs in a pH-dependent manner; that is, NIC has a net positive charge at weakly acidic pH to bind to negatively charged EVs through electrostatic interactions, whereas it has a net negative charge at weakly basic pH to dissociate from EVs by

electrostatic repulsion (Fig. 1A). EV-CaRiS achieved the isolation which was three-fold higher in terms of the number of small EVs with high purity in one-third the time required for UC. Moreover, single-particle analysis of the catch-and-release of small EVs by NIC was performed by labeling the stereotypical exosome marker proteins with antibodies. Overall, these results demonstrated that EV-CaRiS using a NIC is a practical system for the isolation and single-particle observation of small EVs.

Table 1. nFAAV5 and NICs.

Peptide	Sequence[a]	pK_a value of the side chain		Net Charge[b]		Retention Time (min)[c]	Binding property[d]				Ratio[e]		
		Acidic amino acid	Basic amino acid	pH 6	pH 9		pH 6		pH 9		K_d	B (3 μM)	B_{max}
							K_d (μM)	B_{max}	K_d (μM)	B_{max}			
nFAAV5	DKBLLKXLNKBTDBLSKX-GSGSC-NH_2	Asp (3.9)	Lys (10.5)	+2.0	+1.9	18.3	80.5	130.8	116.0	108.6	1.4	1.7	1.2
NIC1	DOBLLOXLNOBTDBLSOX-GSGSC-NH_2	Asp (3.9)	Orn (8.7)	+2.0	−0.7	16.4	3.4	127.2	14.0	186.5	4.1	1.8	0.7
NIC2	DZBLLZXLNZBTDBLSZX-GSGSC-NH_2	Asp (3.9)	Dap (6.7)	+2.0	−0.7	14.8	27.6	211.8	73.3	112.4	2.7	4.7	1.9
NIC3	EOBLLOXLNOBTEBLSOX-GSGSC-NH_2	Glu (4.3)	Orn (8.7)	+0.7	−2.0	16.4	45.8	247.6	140.0	283.2	3.1	2.6	0.9
NIC4	EZBLLZXLNZBTEBLSZX-GSGSC-NH_2	Glu (4.3)	Dap (6.7)	+0.7	−2.0	14.5	51.4	290.0	268.9	180.8	5.2	8.0	1.6

(*a*) The single letters of B, O, X, and Z indicate 2-aminoisobutyric acid, ornithine, norleucine, and 2,3-diaminopropionic acid, respectively. Norleucine was used instead of methionine to prevent the oxidation. The C-termini of all peptides were amidated. (*b*) The net charges of the peptides at pH 6 and 9 not including the charge of the N-terminus. (*c*) The retention time of the NBD-labeled peptides analyzed by RP-HPLC on a COSMOSIL $5C_{18}$-AR-II column (4.6 mm I.D. × 150 mm) using a linear gradient from 30 to 80% acetonitrile in 0.1% aqueous TFA for 30 min at 40 ºC at a flow rate of 1 mL/min (detection at 220 nm). (*d*) The K_d and B_{max} values were determined by fitting the saturation curves (Fig. 1C–G) based on the Langmuir isotherm model. (*e*) The ratios of the K_d, B (3 μM), and B_{max} values at pH 6 to 9 indicate the increment degrees in the binding affinity for liposomes, in the number of peptides bound on the vesicle surface at [L] = 3 μM, and in the plateau level, respectively.

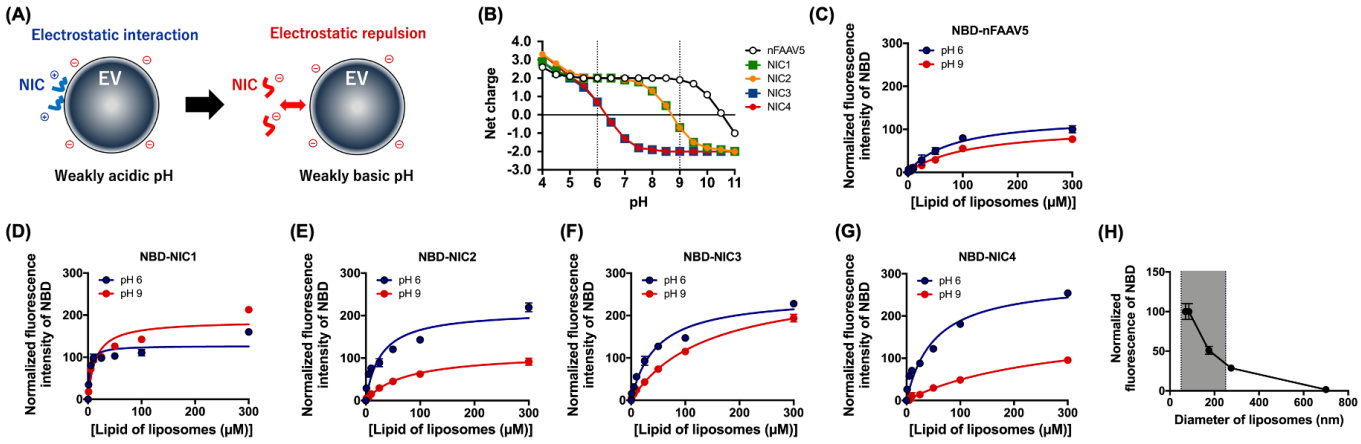

Figure 1. Peptide binding properties. (A) A schematic diagram of the pH-dependent vesicle-binding manner of NICs. (B) A pH-dependent change in the net charge of nFAAV5 and NIC1–NIC4 calculated based on the Henderson-Hasselbalch equation. The binding saturation curves for NBD-nFAAV5 (C), NBD-NIC1 (D), NBD-NIC2 (E), NBD-NIC3 (F), and NBD-NIC4 (G) at pH 6 and 9. The data were normalized by the plateau value of NBD-nFAAV5 and were fitted with Equation (1) to determine the K_d values. (H) The curvature sensitivity of NBD-NIC4. Mean ± S.D., $n = 3$.

MATERIALS AND METHODS

Peptide synthesis. The procedure has been described previously[12]. For single-molecule observation by TIRFM, the N-terminus was labeled with TMR dye by reacting 5-TAMRA *N*-succinimidyl ester (1.2 equiv.) (Tokyo Chemical Industry, Tokyo, Japan) with peptides (1 equiv.) in the presence of DIEA (6 equiv.) on resin for 38 h at 25 ºC. After deprotection and cleavage of peptides from the resin, the peptides were purified by RP-HPLC. For biotinylation, purified TMR-NIC4 was reacted with biotin-PEG2-maleimide (3.5 equiv.) (Tokyo Chemical Industry) in pH-controlled phosphate-buffered saline [PBS(–):137 mM NaCl, 2.7 mM KCl, 8.1 mM Na_2HPO_4, and 1.5 mM KH_2PO_4] (pH 7.4)/acetonitrile (5:2, v/v) at 25ºC for 1 h. The masses of the products were confirmed by matrix-assisted laser desorption ionization time-of-flight mass spectrometry (MALDI-TOF-MS) using AXIMA (Shimadzu, Kyoto, Japan) and electrospray ionization-mass spectrometry (ESI-MS) with LCMS-8040 (Shimadzu).

Liposome binding of peptides. The NBD fluorescence intensity was measured using EnVision (PerkinElmer, Yokohama, Japan) 10 min after peptides mixed liposomes. The K_d values were determined using the following equations[12]:

$$B_C = \frac{B_{max}}{1+\frac{K_d}{c}} \quad (1) \qquad \frac{B_C}{B_{max}} = \frac{F-F_0}{F_t-F_0} \times 100 = \frac{1}{1+\frac{K_d}{c}} \quad (2)$$

where B_c, B_{max}, and c indicate the binding level of the peptides to the vesicles, the maximum level of binding, and the given lipid concentration of the vesicles, respectively. The ratio of $(F - F_0) / (F_t - F_0)$ was calculated and plotted as a function of c, where F_0 and F are the fluorescence intensities of NBD-peptides at each point in

the absence and presence of vesicles, respectively, and F_t indicates the fluorescence intensities of NBD-nFAAV5 at [L] = 300 μM at pH 6.

Cell culture. HeLa and PANC-1 cells were seeded at 2.0×10^6 cells on a culture dish in 10 mL DMEM (high glucose) and 10% (v/v) fetal bovine serum (FBS). MSC-R37 cells[15] (RIKEN BRC, Ibaraki, Japan) were seeded at 2.0×10^5 cells in 10 mL DMEM (low glucose), 3 ng/mL bFGF, and 10% (v/v) FBS. Twenty-four hours after seeding the cells, the cultured medium was removed, and the cells were washed five times with fresh medium. The cells were then incubated for an additional 24 h in 10 mL fresh DMEM (high or low glucose) containing 10% (v/v) exosome-free FBS.

EV isolation by EV-CaRiS. The cell-cultured medium (10 mL) was collected and the pH was adjusted to pH 6 with lactic acid. The pH-controlled medium was transferred into a 15 mL tube containing NIC4-resin of 250 μL in a precipitation volume and incubated with NIC4-resin for 30 min while tapping the tube at 5 min intervals for mixing the resin and media. The flow-through was carefully removed using a pipette and NIC4-resin was washed with a pH 6 buffer five times. Subsequently, a pH 10 buffer (1.0 mL) was added to the resin (final pH ~9) and incubated for 30 min. The supernatant containing EVs was collected using a pipette.

EV isolation by UC. The cell-cultured medium (10 mL) from the cells was collected into a 15 mL tube and centrifuged with an angle rotor at 300 ×*g* at 4 ºC for 10 min using himac CF16RN (Hitachi koki, Tokyo, Japan). The supernatant was sequentially centrifuged at 2,000 ×*g* at 4 ºC for 10 min and at 10,000 or 15,000 ×*g* at 4 ºC for 30 min, and then subjected to ultracentrifugation at 100,000 ×*g* (R_{max}) for 70 min using himac CP80WX and a P70AT2 angle rotor (Hitachi Koki). The pellet was resuspended in 4 mL PBS(–) by pipetting 30 times, and ultracentrifuged again under the same condition. The pellet was resuspended in 1 mL of PBS(–).

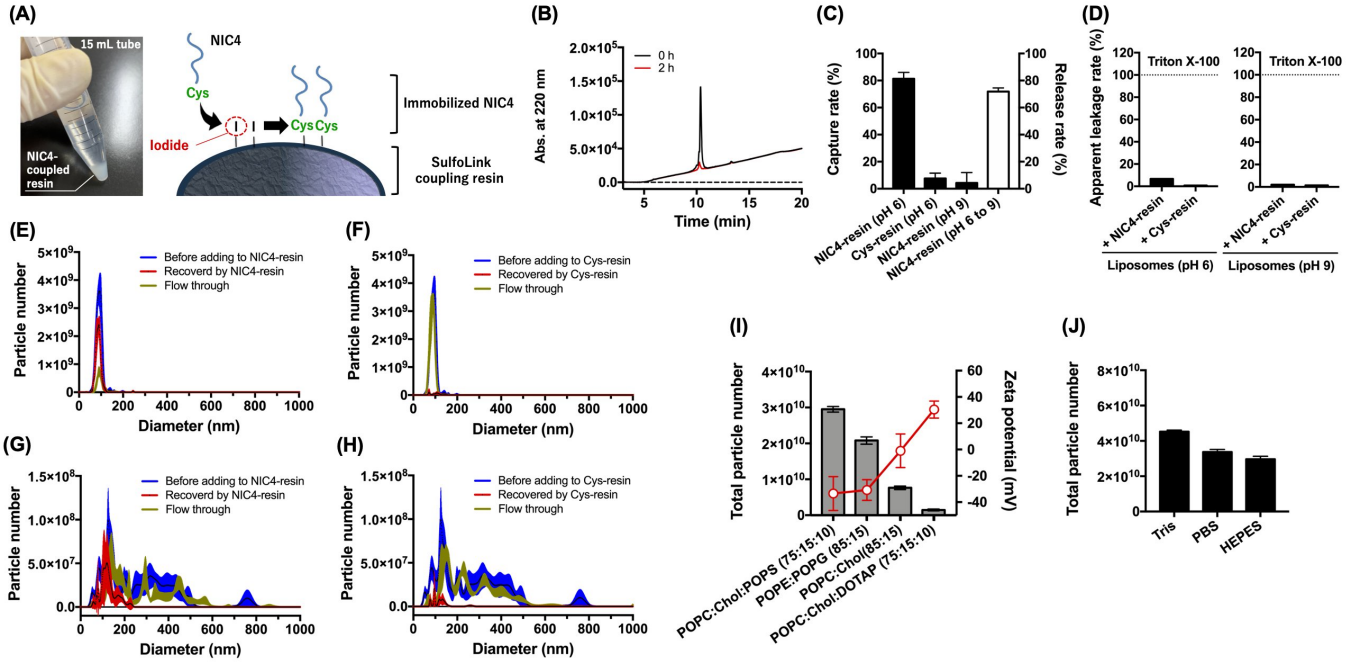

Figure 2. Liposome-recovery abilities of NIC4-resin. (A) A 15 mL tube containing NIC4-resin and a schematic diagram of NIC4 coupling onto the SulfoLink™ resin. (B) The monitoring of the NIC4-coupling reaction based on the absorbance at 220 nm using RP-HPLC. (C) Liposome-capture and -release rates of NIC4-resin and Cys-resin at pH 6 and 9 (mean ± S.D., n = 3). The left and right y-axes show the capture rate (black) and the release rate (white), respectively. The apparent leakage rates of liposomes by NIC4-resin and Cys-resin at pH 6 and pH 9 (D). The recovery of size-homogeneous liposomes by NIC4-resin (E) and Cys-resin (F). The recovery of size-heterogeneous liposomes by NIC4-resin (G) and Cys-resin (H). (I) The relationship between the vesicle binding preference of the peptide and the ζ of liposomes with different lipid compositions (mol%). The bars and lines show the N (left y-axes) and ζ (right y-axes), respectively. POPE: 1-palmitoyl-2-oleoyl-*sn*-glycero-3-phosphoethanolamine, POPG: 1-palmitoyl-2-oleoyl-*sn*-glycero-3-phosphatidylglycerol, DOTAP: 1,2-di-oleoyl-3-trimethylammonium-propane. (J) The N of recovered liposomes (POPC:Chol:POPS = 75:15:10 mol%) using pH-controlled buffers (vesicle-capture and -release was done at pH 6 and 9, respectively). HEPES buffer (25 mM HEPES, 150 mM NaCl).

Table 2. The diameters and N of liposomes.

Vesicle[a]	Diameter of vesicles (nm) (mean ± S.D.)			N of vesicles[b] (mean ± S.D.)			n
	before adding to NIC4-resin	flow through of NIC4-resin	recovered from NIC4-resin	before adding to NIC4-resin	flow through of NIC4-resin	recovered from NIC4-resin	
Size-homogeneous Liposomes	91.2 ± 0.6	95.6 ± 2.4	88.7 ± 0.9	$(5.95 \pm 0.57) \times 10^{10}$	$(1.01 \pm 0.15) \times 10^{10}$	$(3.36 \pm 0.37) \times 10^{10}$	5
Size-heterogeneous Liposomes	265.6 ± 39.7	290.5 ± 10.0	131.2 ± 6.3	$(1.37 \pm 0.11) \times 10^{9}$	$(9.21 \pm 0.05) \times 10^{8}$	$(3.02 \pm 0.57) \times 10^{8}$	5
	before adding to Cys-resin	flow through of Cys-resin	recovered from Cys-resin	before adding to Cys-resin	flow through of Cys-resin	recovered from Cys-resin	
Size-homogeneous Liposomes	91.2 ± 0.6	87.5 ± 1.0	97.9 ± 8.5	$(5.95 \pm 0.57) \times 10^{10}$	$(6.41 \pm 0.86) \times 10^{10}$	$(7.65 \pm 1.77) \times 10^{8}$	5
Size-heterogeneous Liposomes	265.6 ± 39.7	273.3 ± 15.0	140.5 ± 22.4	$(1.37 \pm 0.11) \times 10^{9}$	$(1.15 \pm 0.13) \times 10^{9}$	$(5.33 \pm 1.42) \times 10^{7}$	5

(*a*) Size-homogeneous and -heterogeneous liposomes indicate vesicles extruded and unextruded through the polycarbonate filter with a pore diameter of 50 nm after hydration of the lipid film. (*b*) The diameter and [PN] of liposomes were obtained by NTA. The *N* was calculated by multiplying the [PN] by the total sample volume.

Results

Peptide design and binding property to liposomes. Based on the original peptide nFAAV5[11], we designed pH-responsive NIC1–NIC4 in which a basic amino acid residue, lysine (pK_a value of the side chain: ~10.5), was substituted with ornithine (Orn, pK_a: ~8.7)[16] or 2,3-diaminopropionic acid (Dap, pK_a: ~6.3)[17] (Table 1). NIC3 and 4 were designed to adopt a higher α-helical structure than NIC1 and 2 upon binding to EVs, because an acidic amino acid residue, glutamate (Glu, pK_a: ~4.3) reportedly contributes to the improvement of peptide's α-helicity in comparison with aspartate (Asp, pK_a: ~3.9)[18]. Based on the Henderson-Hasselbalch equation, the net charge of nFAAV5 remains at approximately +2 over the pH range of 6–9, whereas that of NIC1–NIC4 varies from positive to negative (Fig. 1B) (Table 1).

To assess the binding properties of these peptides to vesicles, a liposome-pure system was used for the binding assay. The liposomes used as the EV model[19] were composed of 1-palmitoyl-2-oleoyl-*sn*-glycero-3-phosphocholine (POPC), cholesterol (Chol), and 1-palmitoyl-2-oleoyl-*sn*-glycero-3-phospho-L-serine (POPS) at 75, 15, and 10 mol%, respectively. The diameter and zeta potential (ζ) of the extruded liposomes at pH 6 and 9 were approximately 95.8 ± 0.3 nm and –37.4 ± 2.4 mV and 95.1 ± 0.6 nm and –40.0 ± 3.7 mV, respectively (mean ± S.D., n = 5). There were no significant differences between the diameters or ζ values at pH 6 and 9, according to multiple *t*-tests (significance level: 0.05). The N-termini of the peptides (Table S1 and Figures S1–S5) were labeled with nitrobenzoxadiazole (NBD), a dye that emits strong fluorescence in hydrophobic membrane environments. Peptide binding to the vesicles was evaluated by an increase in NBD fluorescence intensity. NBD-nFAAV5, NBD-NIC1, and 3 exhibited similar binding saturation curves with a small difference between the maximum levels of binding (B_{max}) at pH 6 and 9, whereas NBD-NIC2 and 4 exhibited curves with relatively large gaps (Fig. 1C–G). The dissociation constant (K_d) values at pH 6 and 9 are as shown in Table 1 at a lipid concentration ([L]). These results indicated that the substitution of Lys residues with Dap residues contributes to the pH dependence of vesicle binding of the peptides (Table 1).

To determine the most suitable peptide for EV isolation, the pH-sensitive vesicle binding ability was evaluated based on the ratio of the binding level (B) at [L] = 3 μM at pH 6 to 9 because the particle number concentration ([PN]) of EVs isolated in this study is in an order of approximately 10^9 particles/mL, and nanoparticle tracking analysis (NTA) revealed that liposomes at [L] = 3 μM corresponds to ~3.6×10^9 particles/mL (Fig. S6). NBD-NIC4 was chosen as the best peptide for the catch-and-release of EVs owing to the highest B ratio (8.0) at [L] = 3 μM among the candidates (Table 1). The pH dependence of vesicle binding was also observed for the secondary structure in the presence of liposomes at pH 6 and 9 (*Cf.* Table S2 and Fig. S12 for the further discussion). NIC4 was found to be a suitable peptide for collecting small EVs with a diameter smaller than 250 nm owing to its specific vesicle-binding range. The curvature sensitivity of NBD-NIC4 was examined using extruded liposomes with different diameters at the same [L]. The smaller the liposomes were (as the higher their curvatures were), the higher the fluorescent intensity of NBD-NIC4 exhibited (Fig. 1H and Table S3). This tendency was particularly remarkable for liposomes with diameters smaller than 200 nm, corresponding to the size of small EVs.

Liposome recovery by EV-CaRiS. Non-labeling NIC4 (Table S1 and Fig. S13) was coupled to iodides on the surface of SulfoLink™ coupling resin through a Cys residue at the C-terminus (Fig. 2A). The coupling reaction was monitored by detecting the amount of NIC4 remaining in the supernatant after mixing NIC4 with resin. Two hours after starting the reaction at pH 8, the amount of free NIC4 was remarkably reduced and the reaction was completed (the reaction rate based on the peak area was 91.5 ± 1.3% (mean ± S.D., n = 3)) (Fig. 2B). The NIC4 loading rate was estimated to be 2.16×10^{11} NIC4 / bead under the assumption that the peptide at a reaction rate of 91.5% (~128 nmol) reacted with spherical beads with a diameter of 100 μm (sphere packing rate of beads under a suspending condition: 75%). The liposome-capture and -release rates were precisely determined by quantifying the [L] of phosphatidylcholine (PC) based on an enzymatic fluorometric assay[20, 21] (Fig. S14). A stepwise increase in release capacity depending on pH was observed (Fig. S15) as correlated with the net charge in Figure 1B. Using liposomes with a diameter of 90 nm at [L] = 30 μM, the liposome capture rates of the NIC4-resin at pH 6 and 9 were determined to be 81.4% and 4.3%, respectively (Fig. 2C). In a comparative study, the liposome-capture rate of Cys-resin at pH 6 was 7.6% (Fig. 2C), indicating that NIC4 contributed to pH-dependent liposome capture. The liposome-release rate after changing the pH value to 9 was 71.9%. The capture and release rates were evaluated after a sufficient incubation time (120 min). This was because it took 30 min for free NBD-NIC4 to fully dissociate from the liposomes when the pH was changed from 6 to 9 after it bound to the liposomes at pH 6 (Fig. S16). Next, little disruption of liposomes by NIC4- or Cys-resin was confirmed by the leakage assay either at pH 6 or 9 (Fig. S17 and Fig. 2D).

To examine the total particle number (N) and the particle size distribution of liposomes recovered by EV-CaRiS, size-homogeneous liposomes with an average diameter of 94 nm (a range from 25 to 200 nm) and size-heterogeneous liposomes with an average diameter of 266 nm (a range from 20 to 890 nm) were prepared at [L] of ~30 μM. The N of the size-heterogeneous liposomes at this [L] was close to that of the cell-cultured media, as shown in Table 2. The NTA results for the size-homogeneous liposomes recovered using NIC4-resin and Cys-resin are displayed in Figures 2E and F, respectively. The N of liposomes recovered by NIC4-resin (3.36×10^{10} particles, the recovery rate: 56%) were remarkably higher than that by Cys-resin (7.65×10^8 particles, the recovery rate: 1.3%) (Table 2). The NTA results for the size-heterogeneous liposomes recovered by NIC4-resin and Cys-resin are shown in Figures 2G and H, respectively. The particle sizes of the liposomes recovered using NIC4-resin were less than 200 nm, and the average diameter was 131 nm (Table 2). The N of size-heterogeneous liposomes before and after adding to the NIC4-resin were 1.37×10^9 and 3.02×10^8 particles, respectively (Table 2), and the recovery rate of the liposomes smaller than 200 nm was 51%. In contrast, the N of liposomes recovered by Cys-resin was 5.33×10^7 particles (Table 2), and the recovery rate was 6.8%. The vesicle binding preference of the peptide to liposomes with different lipid compositions was investigated (Fig. 2I), indicating that the electrostatic interaction between the peptide and vesicles plays a key role on the vesicle recovery, but even PS-deficient liposomes (POPC:Chol = 85:15 mol%) were also recovered probably by the hydrophobic interaction. Liposome recovery was successfully done even using three types of pH-controlled buffers (pH 6 and 9) (Fig. 2J). A slight decrease in the recovery suggested that the ion strength of buffers could influence the electrostatic interaction.

EV isolation by EV-CaRiS. EVs secreted from the human cervical cancer cell line (HeLa)[10, 22], the human pancreatic carcinoma cell line (PANC-1)[23, 24], and human bone marrow mesenchymal stem cells (MSC-R37)[25, 26] have been well studied. The EV-isolation

performance of EV-CaRiS was evaluated and compared with a major method UC. The cell-cultured medium (10 mL) was

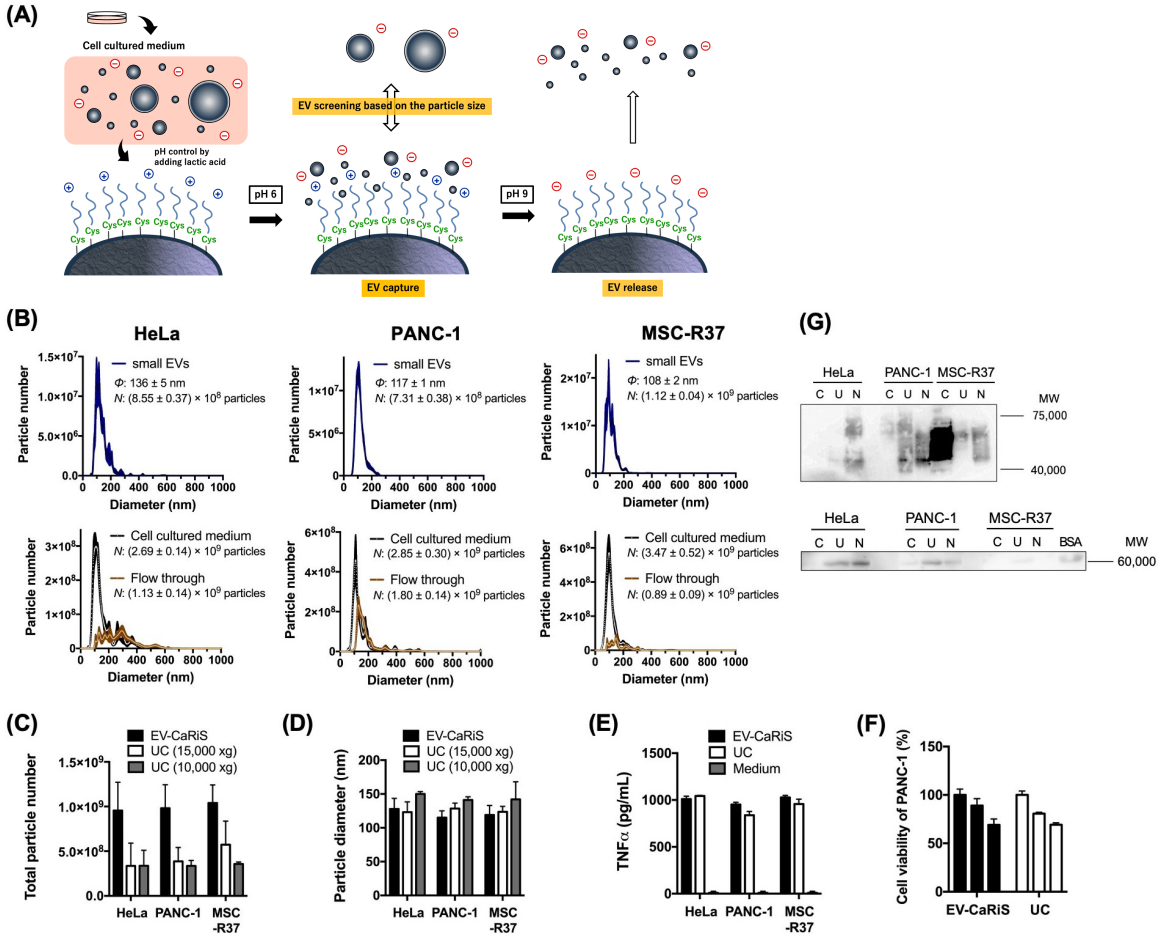

Figure 3. EV-isolation abilities of EV-CaRiS. (A) A schematic diagram of EV-CaRiS by NIC4-resin. 1st step: the pH adjustment to 6 of cell-cultured media with lactic acid. 2nd step: the EV capture by NIC4-resin. 3rd step: wash out of large EVs and proteins, and the EV release from NIC4-resin. (B) The size distributions of the isolated EVs (blue) and particles in cell-cultured media before adding to NIC4-resin (black) and the flow through (brown) of HeLa, PANC-1, and MSC-R37, respectively. The average diameter (φ) and N of the isolated EVs are shown in each panel. A comparison of the N (C) and the diameter of the EVs (D) isolated by EV-CaRiS and UC (mean ± S.D., $n = 3$ or 5). UC (15,000 or 10,000 ×g) means centrifugation conditions to remove larger EVs before ultracentrifugation. Immune-stimulation activities of small EVs from three cell lines (E) ([PN] = 2.5–3.0 × 10^6 particles/mL) and anti-cancer activities of small EVs from MSC-R37 against PANC-1 cells (F) ([PN] = 0, 4.0 × 10^7, 1.6 × 10^8 particles/mL from the left). (G) Western blotting analysis of CD63 and BSA. C, U, N, and BSA indicate cell lysates, UC-isolated EVs, NIC4-resin-isolated EVs, and the standard BSA, respectively. The loading particle number of EVs: 1.3 × 10^8 (HeLa), 1.9 × 10^8 (PANC-1), and 1.8 × 10^8 (MSC-R37). The loading amount: 5.0 μg (cell lysates) and 2.0 μg (standard BSA).

collected from each cell line and its pH was adjusted to 6 by adding 15–30 μL of lactic acid to the collected medium (Fig. 3A); lactic acid itself is naturally observed in a cultured medium as a waste product from cultured cells. The pH-controlled medium was transferred into a 15 mL tube containing NIC4-resin. After incubation to catch the EVs with NIC4-resin, the flow-through was removed. The resin was washed five times with a pH 6 buffer and then treated with a pH 9 buffer to release the EVs from NIC4-resin. When the N of the particles was plotted against the EV capture or release time, the shortest time required to efficiently isolate EVs was determined to be 30 min for EV capture and release, respectively (Fig. S18). The total time including wash steps was approximately 90 min, which is one-third or less than the UC method. To confirm the reproducibility of EV-CaRiS and the number of repeated uses of the same resin, we performed five independent experiments for these three cell lines. As shown in Figure S19, this system was highly reproducible and the same NIC4 resin could be used repeatedly for EV isolation at least five times. The isolated EVs in all data had a diameter of less than 200 nm. In comparison with the cell-cultured media before addition to NIC4-resin, the particle number at a diameter ≤ 200 nm was remarkably reduced in the flow-through (Fig. 3B), indicating that the EVs were collected from the cell-cultured media by NIC4-resin. This trend was also observed in the UC results (Fig. S20). There were no significant differences between the ζ values for the EVs isolated using NIC4-resin and UC (Table S4). The PN distribution of large EVs in flow through (EV-CaRiS) and the pellet (UC) was shown in Figure S21. In contrast, the N of the EVs collected by the NIC4-resin was three-fold higher than that collected by UC (Fig. 3C). The average diameter of the small EVs isolated by EV-CaRiS was similar or slightly smaller than those isolated by UC (Fig. 3D). The EVs isolated by EV-CaRiS and UC exhibited similar immune-stimulation activities (Fig. 3E) against macrophage RAW264.7. Moreover, the isolated EVs from MSC-R37 exerted anti-cancer effects (Fig. 3F) on

PANC-1 cells. Finally, the purity of the collected EVs was evaluated by western blot analysis immunoblotting an universal exosome-marker protein, CD63 and an EV-unrelated major serum protein from FBS, bovine serum albumin (BSA). All the EVs collected from HeLa, PANC-1, and MSC-R37 cells by NIC4-resin exhibited similar CD63 bands with the cell lysate of MSC-R37 used as a positive control (Fig. 3G). The CD63 band appeared over a broad range as previous reports[10, 22, 27]. The band intensities of EVs isolated by EV-CaRiS were higher than those by UC under the same loading particle number. CD63 bands were barely detectable in the HeLa and PANC-1 cell lysates. This was because the number of cells used for the cell lysate was 100-fold lower than that used previously[10]; alternatively, CD63-transfected cells were used for western blotting analysis[22]. The amount of BSA contaminating the EV samples was negligible. Taken together, EV-CaRiS achieved a three-fold higher amount of small-EV isolation with high purity in one-third less time than the UC method.

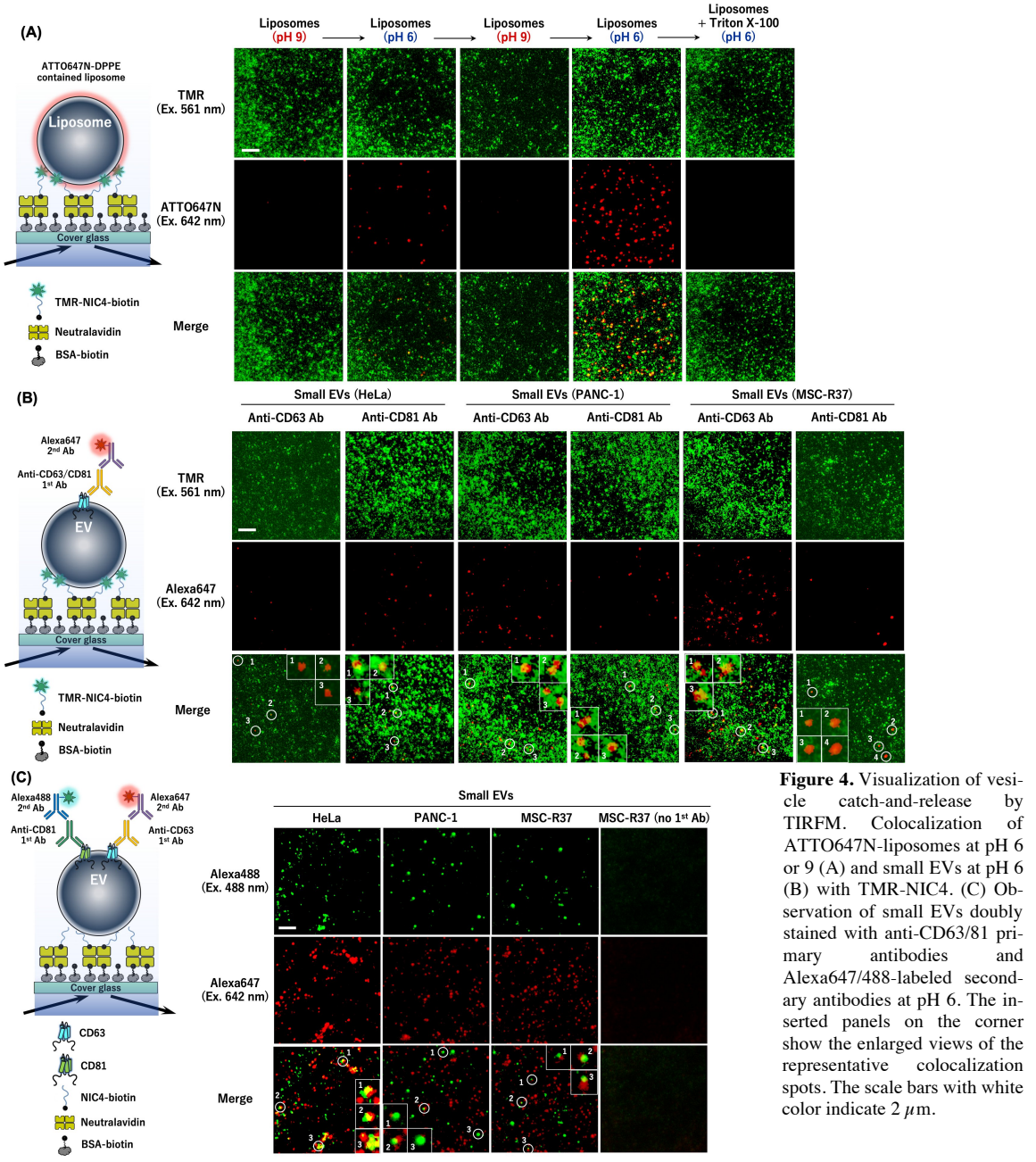

Figure 4. Visualization of vesicle catch-and-release by TIRFM. Colocalization of ATTO647N-liposomes at pH 6 or 9 (A) and small EVs at pH 6 (B) with TMR-NIC4. (C) Observation of small EVs doubly stained with anti-CD63/81 primary antibodies and Alexa647/488-labeled secondary antibodies at pH 6. The inserted panels on the corner show the enlarged views of the representative colocalization spots. The scale bars with white color indicate 2 μm.

Visualization of catch-and-release of vesicles by TIRFM. To visualize the catch-and-release of vesicles by NIC4 with TIRFM, the N-terminus and a Cys residue at the C-terminus of NIC4 were modified with tetramethylrhodamine (TMR) and biotin, respectively (TMR-NIC4-biotin) (Fig. S22). After a cover glass was sequentially coated with BSA-biotin and neutravidin, TMR-NIC4-biotin was immobilized on neutravidin (Fig. 4). Liposomes (POPC:Chol:POPS = 75:15:10 mol%) contained ATTO647N-labeled 1,2-dipalmitoyl-*sn*-glycero-3-phosphoethanolamine (ATTO647N-DPPE) at 0.1 mol%. TMR and ATTO647N are pH-insensitive dyes. Firstly, we confirmed that there was no fluorescence crosstalk between TMR and ATTO647N channels with excitation at 561 and 642 nm, respectively, or no fluorescent signal of ATTO647N directly excited at 561 nm (Fig. S23A). While no ATTO647N-fluorescent spots were observed at pH 9, multiple ATTO647N-fluorescent spots were visualized at pH 6 in the

presence of fluorescent liposomes at [L] = 25 nM, (~3.0×10^7 particles/mL) (Fig. 4A). Colocalization of TMR-NIC4 and ATTO647N-liposomes was observed for all spots, as shown in yellow or orange. When the pH was changed from 6 to 9, the ATTO647N-fluorescent spots disappeared (Fig. 4A). To check the repeated vesicle-binding ability of NIC4, the pH was reversed to 6 again, and vesicle capture was observed in the presence of the liposomes at [L] = 200 nM (~2.4×10^8 particles/mL). In proportion to [L] (or [PN]), the observed ATTO647N-fluorescent spots increased and perfectly colocalized with TMR-fluorescent spots (Fig. 4A). Finally, to verify that the ATTO647N-fluorescent spots colocalized with the TMR-fluorescent spots were lipidic vesicles, the ATTO647N-fluorescent spots were observed in the presence of 0.1% (w/v) Triton X-100 under the same condition. As the result, ATTO647N-fluorescent spots completely disappeared (Fig. 4A). These data demonstrate that NIC4 repeatedly captures and releases lipidic vesicles in a pH-dependent manner.

The catch-and-release of small EVs by NIC4 immobilized on glass was visualized using TIRFM, as illustrated in Figure 4B. The EVs derived from HeLa, PANC-1, and MSC-R37 cells were sequentially incubated with anti-human CD63/CD81 primary antibodies and a pH-stable Alexa Fluor 647-labeled secondary antibody in a pH 6 buffer. The mixture containing the EV particles at [PN] = $1.3–1.9 \times 10^8$ particles/mL was incubated at pH 6, and TMR- and Alexa647-fluorescent imaging were performed. The Alexa647-fluorescent spots were observed for EVs derived from all cell lines incubated with anti-CD63 or CD81 antibodies, and colocalized with TMR-fluorescent spots (Fig. 4B). Notably, no Alexa647-fluorescent spot was observed in the absence of EVs (Fig. S23B), indicating that the Alexa647-fluorescent spots in the presence of EVs were not due to the free antibody present in the solution. In addition, Alexa647-fluorescent spots almost completely disappeared at pH 9 (Fig. S24) or in the presence of 1.0% (w/v) Triton X-100 at pH 6 (Fig. S25), demonstrating that NIC4 can also be used to capture and release biogenic lipid vesicles in a pH-dependent manner. We also observed small EVs doubly stained with anti-CD63/81 antibodies and their fluorescent secondary antibodies on the non-labeling NIC4-biotin coated glass (Fig. 4C and S26). Small EVs partially exhibited the dual color, indicating that some of small EVs isolated by EV-CaRiS contained both CD63/81 biomarkers.

Discussion. A wide variety of elegant strategies for EV isolation have been developed so far, including conventional UC, sequential centrifugal ultrafiltration (SCUF)[9], dual-mode chromatography (DMC)[27], affinity purification (AP)[28], polymer-based precipitation (PBP)[29], tangential flow filtration-size exclusion chromatography (TFF-SEC)[30], phosphatidylserine (PS) capture[31], and so on. Even though no matter how remarkable the technology is for EV isolation, the technology may be too advanced to reproduce or reconstruct for all laboratories. Therefore, these issues probably make it difficult for researchers to establish gold standard EV isolation methods and to compare experimental data between different laboratories.

In comparison with existing strategies, the leading point of our EV-CaRiS is that it does not require any specialized experimental equipment and can reproducibly isolate EVs with high purity from a small amount of cell-cultured media (10 mL) in a relatively short time (~1.5 h). For instance, the UC method requires different types of centrifuges and ultracentrifuges at each step, in addition to special rotors. Specialized experimental equipment carries the financial risk of high costs of installations and repair. TFF-SEC achieved an EV isolation of 11–27-fold higher particle number than UC, whereas 20–30% of particles had a large size > 200 nm and albumin content was non-negligible. The SCUF method requires 900 mL of medium for EV isolation. The heparin AP method utilizes EV-interactive heparin agarose beads to isolate EVs using high salt content, and DMC uses an integrated column of SEC and cation-exchange in tandem to isolate high-purity EVs; however, these two methods require several days for EV isolation or 100-fold high cell numbers than EV-CaRiS. For PBP, synthetic polymers need to be removed after EV isolation in cases where they influence downstream experiments. PS capture is an affinity-based method for purifying PS-rich EVs in a Ca^{2+}-dependent manner and can complete the purification within 3–3.5 h. PS plays a key role in negatively charging EVs[32]. EV-CaRiS probably can isolate PS-deficient EVs through the hydrophobic interaction between NIC4 and EVs because PS-free liposomes were recovered by EV-CaRiS (Fig. 2I).

The number of EVs isolated by the UC method was lower than that isolated by EV-CaRiS due to that the small EV pellet is resuspended in buffer for washing non-EV proteins and subjected to ultracentrifugation again. A previous study[8] pointed out that this step is unavoidable for increasing the purity of isolated EVs but it also reduces the quantity of EVs as a trade-off relationship. Indeed, a remarkable decrease in the particle amount between the first and second ultracentrifugation steps was observed (Figure S20). Moreover, there is a technical limitation in completely removing the medium and the purity of EVs is inevitably low. In contrast, a high efficiency of EV isolation achieved by EV-CaRiS is attributed to the amount of the NIC4-resin, meaning that an increase in the resin amount will inevitably increase the amount of EVs. Because multiple peptides bind to a single vesicle through multipoint interactions, the vesicles are strongly captured on the resin at pH 6.

EVs with a diameter of 50–200 nm are within the overlapping size range of exosomes and microvesicles. The experimental data in the present study suggest that EV-CaRiS mainly recovers exosomes. One of the most ubiquitous exosome markers CD63 independent of the secretory pathway[6] was detected by western blot analysis (Fig. 3). EVs containing CD63 and CD81 were observed by single-molecule imaging (Fig. 4). Therefore, we concluded that the majority of EV populations isolated by EV-CaRiS were exosomes. Although an EVs on-chip array using membrane-binding peptides has been previously reported[33], our methodology differs from it at the point that the trapping and dissociation of EVs from NIC4 can be arbitrarily controlled in a pH-dependent manner under mild conditions without destruction. The utility of NIC4 is not limited to EV isolation but also to be applied for a chip array method and single-particle analysis.

Conclusions. A simple and convenient method for EV isolation is desired. In the present study, we demonstrated that EV-CaRiS can reproducibly isolate EVs with high purity from small-scale cell-cultured media (10 mL) in a relatively short time (~1.5 h), without requiring any specialized and expensive experimental equipment. NIC4 allowed efficient EV isolation with resin in a batch method and single-particle observation with TIRFM. The trapping and dissociation of EVs from NIC4 can be arbitrarily controlled because NIC4 reversibly captures and releases EVs in a pH-dependent manner. EVs trapped by NIC4 can be recovered under mild conditions without destruction. The utility of NIC4 is not limited to EV isolation but is also promising for applications of a chip array method and single-particle analysis.

ASSOCIATED CONTENT

Supporting Information

The Supporting Information is available free of charge at https://XXXX.
Experimental details, materials, HPLC profiles and mass analyses, CD spectra, standard curve of PC, binding ability of NBD-NIC4, leakage assay of liposomes, NTA of EVs isolated by UC, Observation of EVs by TIRFM (PDF).

AUTHOR INFORMATION

Corresponding Author

Kenichi Kawano – Graduate School of Pharmaceutical Sciences, Kyoto University, Kyoto 606-8501, Japan. orcid.org/0000-0003-1927-2922; *E-mail: kawano.kenichi.2u@kyoto-u.ac.jp

Authors

Yuki Kuzuma – Graduate School of Pharmaceutical Sciences, Kyoto University, Kyoto 606-8501, Japan.

Koichi Yoshio – Graduate School of Pharmaceutical Sciences, Kyoto University, Kyoto 606-8501, Japan.

Kenta Hosokawa – Graduate School of Pharmaceutical Sciences, Kyoto University, Kyoto 606-8501, Japan.

Yuuto Oosugi – Graduate School of Pharmaceutical Sciences, Kyoto University, Kyoto 606-8501, Japan.

Takahiro Fujiwara – Institute for Integrated Cell-Material Sciences (WPI-iCeMS), Kyoto University, Kyoto 606-8501, Japan. orcid.org/0000-0001-5576-759X

Fumiaki Yokoyama – Graduate School of Science, The University of Tokyo, Tokyo 113-0033, Japan. orcid.org/0000-0002-4139-4072

Katsumi Matsuzaki – Graduate School of Pharmaceutical Sciences, Kyoto University, Kyoto 606-8501, Japan. orcid.org/0000-0002-0182-1690

Author contributions

K.K.: Conceptualization, Resources, Funding acquisition, Project administration, Investigation, Methodology, Data curation, Formal analysis, Writing – original draft, Writing – review and editing, Visualization, Supervision. **Y.K.**: Investigation, Data curation, Writing – review and editing. **K.Y., K.H., and Y.O.**: Investigation. **T.F.**: Resources, Writing – review & editing, Supervision. **F.Y.**: Conceptualization, Writing – review and editing. **K.M.**: Conceptualization, Resources, Writing – review and editing, Supervision.

Notes

The authors declare no competing interests in relation to this study.

ACKNOWLEDGMENT

This study was financially supported by the Chubei Itoh Foundation (K.K.) and JSPS KAKENHI (21K15254 to K.K.). The authors sincerely thank Prof. Dr. Shin-ya Morita (Shiga University of Medical Science Hospital) for his valuable advice on the enzymatic measurement of PC. The authors express our sincere gratitude to Prof. Dr. Ikuhiko Nakase (Osaka Metropolitan University) for his kind guidance and valuable advice regarding EV isolation using UC. We thank Prof. Dr. Yukio Kato (Hiroshima University) for providing the MSC-R37 cells.

REFERENCES

1. Schwechheimer, C.; Kuehn, M. J., Outer-membrane vesicles from Gram-negative bacteria: biogenesis and functions. *Nat. Rev. Microbiol.* **2015,** *13*, 605–619.
2. Mathieu, M.; Martin-Jaular, L.; Lavieu, G.; Thery, C., Specificities of secretion and uptake of exosomes and other extracellular vesicles for cell-to-cell communication. *Nat. Cell Biol.* **2019,** *21*, 9–17.
3. Pegtel, D. M.; Cosmopoulos, K.; Thorley-Lawson, D. A.; van Eijndhoven, M. A.; Hopmans, E. S.; Lindenberg, J. L.; de Gruijl, T. D.; Wurdinger, T.; Middeldorp, J. M., Functional delivery of viral miRNAs via exosomes. *Proc. Natl. Acad. Sci. U. S. A.* **2010,** *107*, 6328–6333.
4. Record, M.; Carayon, K.; Poirot, M.; Silvente-Poirot, S., Exosomes as new vesicular lipid transporters involved in cell-cell communication and various pathophysiologies. *Biochim. Biophys. Acta.* **2014,** *1841*, 108–120.
5. S, E. L. A.; Mager, I.; Breakefield, X. O.; Wood, M. J., Extracellular vesicles: biology and emerging therapeutic opportunities. *Nat. Rev. Drug Discov.* **2013,** *12*, 347–357.
6. Xu, R.; Greening, D. W.; Zhu, H. J.; Takahashi, N.; Simpson, R. J., Extracellular vesicle isolation and characterization: toward clinical application. *J. Clin. Invest.* **2016,** *126*, 1152–1162.
7. Jeppesen, D. K.; Zhang, Q.; Franklin, J. L.; Coffey, R. J., Extracellular vesicles and nanoparticles: emerging complexities. *Trends Cell Biol.* **2023,** *33*, 667–681.
8. Konoshenko, M. Y.; Lekchnov, E. A.; Vlassov, A. V.; Laktionov, P. P., Isolation of Extracellular Vesicles: General Methodologies and Latest Trends. *Biomed. Res. Int.* **2018,** *2018*, 8545347.
9. Xu, R.; Greening, D. W.; Rai, A.; Ji, H.; Simpson, R. J., Highly-purified exosomes and shed microvesicles isolated from the human colon cancer cell line LIM1863 by sequential centrifugal ultrafiltration are biochemically and functionally distinct. *Methods* **2015,** *87*, 11–25.
10. Mathieu, M.; Nevo, N.; Jouve, M.; Valenzuela, J. I.; Maurin, M.; Verweij, F. J.; Palmulli, R.; Lankar, D.; Dingli, F.; Loew, D.; Rubinstein, E.; Boncompain, G.; Perez, F.; Thery, C., Specificities of exosome versus small ectosome secretion revealed by live intracellular tracking of CD63 and CD9. *Nat. Commun.* **2021,** *12*, 4389.
11. Kawano, K.; Yokoyama, F.; Kamasaka, K.; Kawamoto, J.; Ogawa, T.; Kurihara, T.; Futaki, S., Design of the N-terminus substituted curvature-sensing peptides that exhibit highly sensitive detection ability of bacterial extracellular vesicles. *Chem. Pharm. Bull.* **2021,** *69*, 1075–1082.
12. Kawano, K.; Kamasaka, K.; Yokoyama, F.; Kawamoto, J.; Ogawa, T.; Kurihara, T.; Matsuzaki, K., Structural factors governing binding of curvature-sensing peptides to bacterial extracellular vesicles covered with hydrophilic polysaccharide chains. *Biophys. Chem.* **2023,** *299*, 107039.
13. Bhatia, V. K.; Madsen, K. L.; Bolinger, P. Y.; Kunding, A.; Hedegard, P.; Gether, U.; Stamou, D., Amphipathic motifs in BAR domains are essential for membrane curvature sensing. *EMBO J.* **2009,** *28*, 3303–3314.
14. Kawano, K.; Yokoyama, F.; Kawamoto, J.; Ogawa, T.; Kurihara, T.; Futaki, S., Development of a simple and rapid method for *in situ* vesicle detection in cultured media. *J. Mol. Biol.* **2020,** *432*, 5876–5888.
15. Tsutsumi, S.; Shimazu, A.; Miyazaki, K.; Pan, H.; Koike, C.; Yoshida, E.; Takagishi, K.; Kato, Y., Retention of multilineage differentiation potential of mesenchymal cells during proliferation in response to FGF. *Biochem. Biophys. Res. Commun.* **2001,** *288*, 413–419.
16. Goldsmith, J. O.; Lee, S.; Zambidis, I.; Kuo, L. C., Control of L-ornithine specificity in Escherichia coli ornithine transcarbamoylase. Site-directed mutagenic and pH studies. *J. Biol. Chem.* **1991,** *266*, 18626–18634.
17. Lan, Y.; Langlet-Bertin, B.; Abbate, V.; Vermeer, L. S.; Kong, X.; Sullivan, K. E.; Leborgne, C.; Scherman, D.; Hider, R. C.; Drake, A. F.; Bansal, S. S.; Kichler, A.; Mason, A. J., Incorporation of 2,3-diaminopropionic acid into linear cationic amphipathic peptides produces pH-sensitive vectors. *Chembiochem* **2010,** *11*, 1266–1272.
18. Merutka, G.; Stellwagen, E., Effect of amino acid ion pairs on peptide helicity. *Biochemistry* **1991,** *30*, 1591–1594.
19. Skotland, T.; Hessvik, N. P.; Sandvig, K.; Llorente, A., Exosomal lipid composition and the role of ether lipids and phosphoinositides in exosome biology. *J. Lipid Res.* **2019,** *60*, 9–18.
20. Morita, S. Y.; Tsuji, T.; Terada, T., Protocols for Enzymatic Fluorometric Assays to Quantify Phospholipid Classes. *Int. J. Mol. Sci.* **2020,** *21*, 1032.
21. Morita, S. Y.; Takeuchi, A.; Kitagawa, S., Functional analysis of two isoforms of phosphatidylethanolamine N-methyltransferase. *Biochem. J.* **2010,** *432*, 387–398.
22. Verweij, F. J.; Bebelman, M. P.; Jimenez, C. R.; Garcia-Vallejo, J. J.; Janssen, H.; Neefjes, J.; Knol, J. C.; de Goeij-de Haas, R.; Piersma, S. R.; Baglio, S. R.; Verhage, M.; Middeldorp, J. M.; Zomer, A.; van Rheenen, J.; Coppolino, M. G.; Hurbain, I.; Raposo, G.; Smit, M. J.; Toonen, R. F. G.; van Niel, G.; Pegtel, D. M., Quantifying exosome secretion from single cells reveals a modulatory role for GPCR signaling. *J. Cell Biol.* **2018,** *217*, 1129–1142.
23. Fan, J.; Wei, Q.; Koay, E. J.; Liu, Y.; Ning, B.; Bernard, P. W.; Zhang, N.; Han, H.; Katz, M. H.; Zhao, Z.; Hu, Y., Chemoresistance Transmission via Exosome-Mediated EphA2 Transfer in Pancreatic Cancer. *Theranostics* **2018,** *8*, 5986–5994.
24. Al Faruque, H.; Choi, E. S.; Kim, J. H.; Kim, E., Enhanced effect of autologous EVs delivering paclitaxel in pancreatic cancer. *J. Control Release* **2022,** *347*, 330–346.
25. Li, H.; Li, F., Exosomes from BM-MSCs increase the population of CSCs via transfer of miR-142-3p. *Br. J. Cancer.* **2018,** *119*, 744–755.
26. Ono, M.; Kosaka, N.; Tominaga, N.; Yoshioka, Y.; Takeshita, F.; Takahashi, R. U.; Yoshida, M.; Tsuda, H.; Tamura, K.; Ochiya, T., Exosomes from bone marrow mesenchymal stem cells contain a microRNA that promotes dormancy in metastatic breast cancer cells. *Sci. Signal.* **2014,** *7*, ra63.

27. Van Deun, J.; Jo, A.; Li, H.; Lin, H. Y.; Weissleder, R.; Im, H.; Lee, H., Integrated Dual-Mode Chromatography to Enrich Extracellular Vesicles from Plasma. *Adv. Biosyst.* **2020,** *4*, e1900310.
28. Balaj, L.; Atai, N. A.; Chen, W.; Mu, D.; Tannous, B. A.; Breakefield, X. O.; Skog, J.; Maguire, C. A., Heparin affinity purification of extracellular vesicles. *Sci. Rep.* **2015,** *5*, 10266.
29. Niu, Z.; Pang, R. T. K.; Liu, W.; Li, Q.; Cheng, R.; Yeung, W. S. B., Polymer-based precipitation preserves biological activities of extracellular vesicles from an endometrial cell line. *PLoS One* **2017,** *12*, e0186534.
30. Visan, K. S.; Lobb, R. J.; Ham, S.; Lima, L. G.; Palma, C.; Edna, C. P. Z.; Wu, L. Y.; Gowda, H.; Datta, K. K.; Hartel, G.; Salomon, C.; Moller, A., Comparative analysis of tangential flow filtration and ultracentrifugation, both combined with subsequent size exclusion chromatography, for the isolation of small extracellular vesicles. *J. Extracell. Vesicles* **2022,** *11*, e12266.
31. Nakai, W.; Yoshida, T.; Diez, D.; Miyatake, Y.; Nishibu, T.; Imawaka, N.; Naruse, K.; Sadamura, Y.; Hanayama, R., A novel affinity-based method for the isolation of highly purified extracellular vesicles. *Sci. Rep.* **2016,** *6*, 33935.
32. Matsumoto, A.; Takahashi, Y.; Ogata, K.; Kitamura, S.; Nakagawa, N.; Yamamoto, A.; Ishihama, Y.; Takakura, Y., Phosphatidylserine-deficient small extracellular vesicle is a major somatic cell-derived sEV subpopulation in blood. *iScience* **2021,** *24*, 102839.
33. Gori, A.; Romanato, A.; Greta, B.; Strada, A.; Gagni, P.; Frigerio, R.; Brambilla, D.; Vago, R.; Galbiati, S.; Picciolini, S.; Bedoni, M.; Daaboul, G. G.; Chiari, M.; Cretich, M., Membrane-binding peptides for extracellular vesicles on-chip analysis. *J. Extracell. Vesicles* **2020,** *9*, 1751428.